

Electronic Supplementary Information (ESI)

Probing heat generation and release in 57.5 Ah high-energy-density Li-ion pouch cell with nickel-rich cathode and SiO_x/graphite anode

Xiaopeng Qi,^{a,c} Bingxue Liu,^{a,c} Fengling Yun,^{a,c} Changhong Wang,^b Rennian Wang,^{a,c} Jing Pang,^{a,c,d} Haibo Tang,^{a,c} Wei Quan,^{a,c} Qiang Zhang,^{a,c} Man Yang,^{a,c} Shuaijin Wu,^{a,c} Jiantao Wang^{,a,c,d} and Xueliang Sun^{*,b}*

^a China Automotive Battery Research Institute Co., Ltd., No.11 Xingke Dong Street, Huairou District, Beijing, 101407, China.

^b Department of Mechanical and Materials Engineering, University of Western Ontario, 1151 Richmond St, London, Ontario, N6A 3K7, Canada.

^c GRINM GROUP CORPORATION LIMITED (GRINM Group), No.2 Xijiekou Wai Street, Xicheng District, Beijing, 100088, China.

^d General Research Institute for Nonferrous Metals, No.2 Xijiekou Wai Street, Xicheng District, Beijing, 100088, China.

* Corresponding email: wangjt@glabat.com and xsun9@uwo.ca

1. Experimental section

1.1. Additional cell parameters

The NCM cathode material: The NCM cathode material delivers a 1/3 C discharge capacity of 193.9 mAh g⁻¹ in coin cell test, **Fig. S1**.

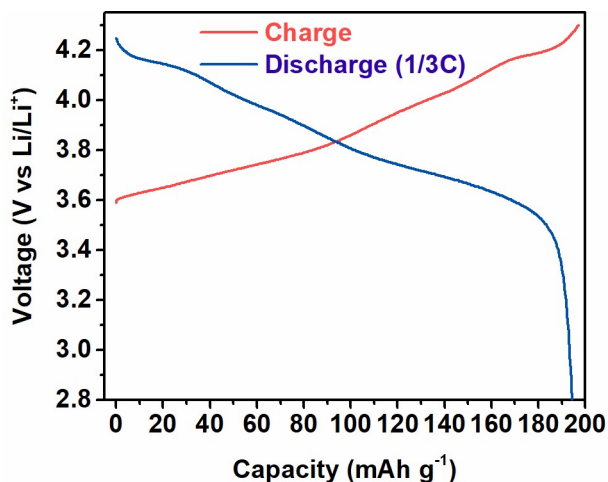


Fig. S1. Charge/discharge voltage curves of the NCM cathode material measured in coin cell test within a voltage window of 4.25-2.8 V.

The electrode laminate parameters: The positive laminates employ current collectors of 15 μm Al foils, are $131 \pm 3 \mu\text{m}$ in thicknesses and 3.36 g cm^{-3} in compaction density. The negative laminates use 6 μm Cu foils as the current collectors, are $123 \pm 3 \mu\text{m}$ thick and 1.56 g cm^{-3} in compaction density.

Cell SOC definition and adjusting method : Standardized CC-CV method (1 C rate charging to 4.2 V followed by constant-voltage charging to 0.05 C) was used to fully charge the cells (100% SOC). Under 1/3 C rate discharging and with a voltage cut-off of 2.8 V, the cell delivered an energy density of 266.9 Wh kg^{-1} and a capacity of 57.5 Ah. Cell SOC's were adjusted by discharging fully charged cells (100% SOC) by proportional capacities on basis of that under the 1/3 discharge.

1.2. Entropic coefficient determination method

Entropic coefficients were measured by the potentiometry method. The cell was placed in a testing chamber and connected to a battery tester for SOC adjusting and voltage monitoring. At each SOC, the chamber temperature was stepped from 0 °C to 10, 20, 30, and 40 °C with a wait time of 3 hours for each step. The entropic coefficients were calculated by dividing the averaged voltage variation in response to the four temperature steps by the amplitude of the temperature step (10°C).

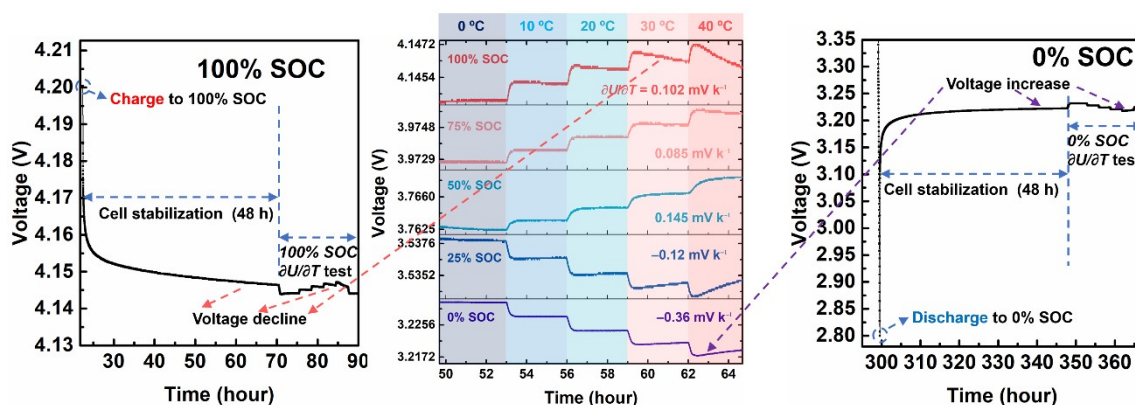


Fig. S2. Voltage curves of the cell at stabilization and temperature-stepping periods during entropic tests. The sloped voltage curves during the entropic coefficient tests, especially those at high temperatures like 30 °C and 40 °C, are mainly due to cell rebalancing, which is generally a time-consuming process. As can be seen in **Fig. S2**, even the cell was allowed for stabilization for 48 hours before the entropic coefficient tests, the cell voltages were still nonstationary. The downward or upward sloping features during the entropic tests are consistent with the previous voltage varying trends (decline or increase) before the entropic tests. Cell self-discharge at high SOC, which is generally inevitable, may also have played a role in the voltage decline at the 100% and 75% SOC. This is also the reason that we did not use excessively prolonged stabilization periods. High temperatures accelerate both the cell rebalancing and the cell self-discharge, and thus caused more sloped voltage curves at elevated temperatures.

1.3. Electrochemical impedance spectroscopy (EIS) tests

EIS tests were performed using a VMP3B potentiostat from BioLogic with a 5 mV stimulation and a frequency range of 0.01 Hz-1 kHz. Data fitting were performed using Zsim implanted in the EC-Lab software V11.25.

1.4. Isothermal calorimeter tests

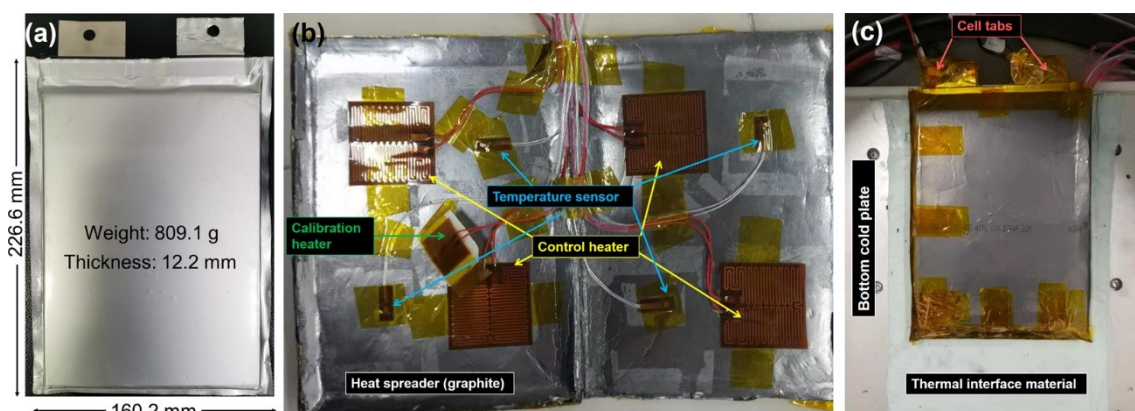


Fig. S3. (a) Dimensions and an image of the testing cell; (b) An image of the graphite heat spreader used in the isothermal calorimeter test containing the temperature sensors, control heaters, and calibration heaters; (c) An image of the cell encapsulated in the heat spreader placed on the bottom cold plate ready for the test.

Heat release characteristics of the cell were investigated using an iso-BTC(500) isothermal calorimeter (IC) from H.E.L Ltd based on power compensation. Before the test, the testing cell was first wrapped by a highly thermal conductive graphite heat spreader containing the temperature sensors, control heaters, and calibration heaters distributed on it (**Fig. S3b**). The heat spreader is to maximize the contact area between the heaters and the cell and to minimize the temperature difference across the cell surface. The heat spreader with the cell was then placed between two cold plates (**Fig. S3c**, top cold plate not shown) with continuous cold oil flowing through them providing a *background temperature* of 5 or 10 °C in our tests. The *cell temperature* (measured by the four temperature sensors) was controlled by the control heater to a preset value of 25 °C, which is also the target of most of the battery thermal management systems. The temperature difference between the cold plates and the cell is referred to as the *compensation drop*, which was selected so that the baseline power of the control heaters is greater than the largest heat expected from the cell.

During the test, the key variable under examination is the electrical power output of the control heaters. Heat generation from the cell will tend to increase the cell temperature and in turn, will result in the control system decreasing the output of the control heaters. If the temperature were uniform within the cell and were precisely controlled at the preset temperature (25 °C in our case), the decrease in control heater power is proportional to the heat generated by the cell. The constant of proportionality (referred to as the efficiency) can be readily determined by the calibration process, during which a calibration heater with known power output is used to simulate cell heat generation and the response of the control heaters is monitored.

However, in practice, and especially when the heat generation rate of the cell is high and the heat conduction within the cell is not sufficiently high, surface temperature variation and temperature difference within the cell is inevitable. Part of the heat generated is absorbed by the cell itself elevating its temperature, and this portion of heat cannot be timely captured by the control heaters. In these cases, what the isothermal calorimeter is measuring is the residue part of the heat, i.e., the heat release power. Because cell surface temperature variation is available during the test, we can include this part heat and adjust the measured heat release rate by adding $mC_p(\partial T/\partial t)$, where $\partial T/\partial t$ is the temperature variation rate and C_p is the specific heat capacity of the cell. The difference between the theoretically calculated heat generation rate and the measured heat release rate after this adjustment would therefore represent the heat absorbed by the cell after the deduction of the surface (or background) temperature variation effect, which we called “heat accumulated” in this study.

1.5. Heat capacity test

The specific heat capacity of the cell was tested by an EV+ accelerating rate calorimeter (THT), which can provide an adiabatic condition. A control heater with known output power was sandwiched between two cells and was used to inject a known amount of heat. The temperature response of the cells was monitored to calculate the specific heat capacity by eqn (S1).

$$C_p = Q/(m\Delta T) \quad (S1)$$

2. Additional experimental results

2.1. Transient behaviors of cell voltage under 1 C discharge

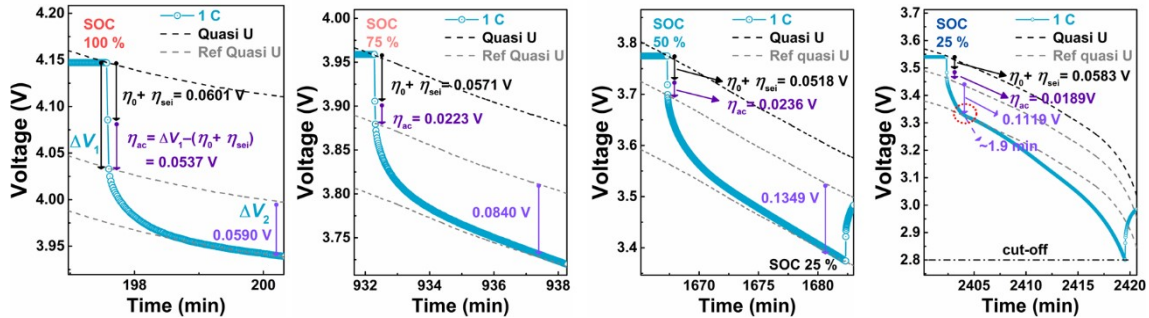


Fig. S4. Transient behaviors of cell voltage under 1 C intermittent discharge at 100%, 75%, 50%, and 25% SOC.

2.2 Heat generation and release study on a cell after long cycles

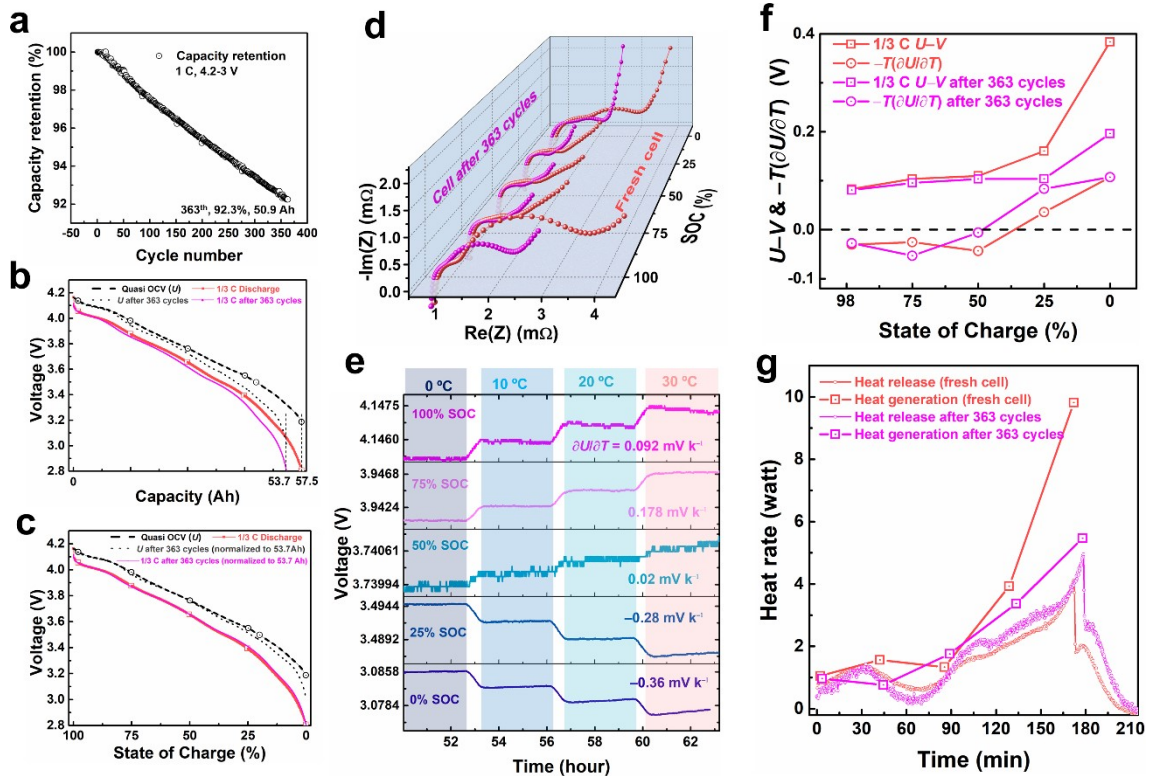


Fig. S5. (a) Cycling performance of the cell; voltage curves of the fresh cell and cycled cell plotted against (b) discharge capacity and (c) state of charge (normalized to discharge capacities); (d) comparison of the Nyquist plots of the fresh cell and the cycled cell; (e) voltage responses of the cycled cell during the entropic coefficient test; (f) comparison of overpotentials and entropic-effect equivalents; (g) comparison of heat generation and release of the fresh cell and the cycled cell.

The cell exhibited excellent cycling performance, recording a capacity retention of 92.3% after 363 cycles (Fig. S5a). As shown in **Fig. S5b**, as the voltage is plotted against the discharge capacity, the OCV and the discharge voltage of the cycled cell both decrease notably, from medium to low SOC, compared to the fresh cell. The cell capacity loss and voltage decline could be attributed to degradation of the SiO_x , which is an alloying-mechanism anode material, featured with huge volumetric charges leading to pulverization and active mass loss, and discharge at a lower voltage compared to graphite.¹

When the cell SOC is normalized to the remaining capacity (Fig. S5b), it can be found that the OCV only decreases slightly at lower SOC. Theoretically, capacity shrinking due to active mass loss from the SiO_x with a lower discharge voltage level would not decrease the cell OCV. The OCV decrease at lower SOC may arise from crystallographic structure variation of the cycled SiO_x which affects its thermodynamic equilibrium potential. Lithiation/delithiation of SiO_x involve various phase changes and SiO_x becomes a complicated mixture of Si clusters, Li_xO , and silicates matrix after cycling.¹ Interestingly, the cell discharge voltage does not decline like the OCV, and even becomes slightly higher than that of the fresh cell at lower SOC. This leads to smaller polarization potentials and polarization heat (Fig. S5f). It also suggests better cell kinetics, which was further investigated by the EIS study in Fig. S5d, showing that both the ohmic and charge transfer resistances decreased after cycling. We believe that these advantageous effects could stem from the volumetric effects of the SiO_x .¹ Expansion and deformation of the SiO_x in the confined electrode space could improve the electric conduction by increasing area contact between particles, thus leading to decreased ohmic resistances. On the other hand, pulverization of the SiO_x could lead to smaller particles and more exposed electroactive surface, rendering the decreased charge transfer resistances. Of course, these beneficial effects may only exist when SiO_x degradation occurs at modest levels and are at the cost of capacity loss.

Entropic coefficients at certain SOC (75%, 50%, 0% SOC) after cycling also deviate notably from those of the fresh cell (Fig. S5e), which could also be attributed to structure variation of the SiO_x . The heat release characteristic of the cycled cell is much like that of the fresh cell, except for the more significant fluctuation of heat release rates at some SOC, which are consistent with the in-step changes of entropic heat. The larger heat release rate of the cycled cell at low SOC may be due to larger exothermic entropic effects that were not fully reflected by the few entropic coefficient data.

References

- 1 T. Chen, J. Wu, Q. L. Zhang and X. Su, *J. Power Sources*, 2017, **363**, 126-144.